PHYSICAL REVIEW B VOLUME 61, NUMBER 14 1 APRIL 2000-II

Oxygen-ordering superstructures in $NdBa_2Cu_3O_{6.5}$ single crystals investigated by hard-x-ray diffraction

T. Frello, N. H. Andersen, J. Madsen, and A. B. Abrahamsen
Condensed Matter Physics and Chemistry Department, Risø National Laboratory, DK-4000 Roskilde, Denmark

M. v. Zimmermann, T. Niemöller, and J. R. Schneider
Hamburger Synchrotronstrahlungslabor HASYLAB am Deutsches Elektronen-Synchrotron DESY, Notkestraße 85, D-22603 Hamburg, Germany

Th. Wolf
Forschungszentrum Karlsruhe, Institut für Technische Physik, D-76021 Karlsruhe, Germany

(Received 6 December 1999)

Single crystals of $NdBa_2Cu_3O_{6+x}$ and $LaBa_2Cu_3O_{6+x}$ at oxygen concentrations $x \approx 0.4$, 0.5, and 0.76 have been investigated by hard-x-ray diffraction. Intricate oxygen superstructures are found in nonsuperconducting $NdBa_2Cu_3O_{6.5}$ crystals. By numerical calculations we demonstrate that three unique coexisting oxygen configurations are required to obtain the observed diffraction pattern. The oxygen configurations found are unlikely to give rise to hole doping of the CuO_2 planes, explaining why a higher oxygen doping is necessary in $NdBa_2Cu_3O_{6+x}$ than in $YBa_2Cu_3O_{6+x}$ to make the compound superconducting.

For all the superconducting $RBa_2Cu_3O_{6+x}$ (R-123) high-T_c cuprates (R=rare earths except Pr, Ce, Tb), the superconducting transition temperature T_c depends strongly on the oxygen concentration x. In the best studied compound $YBa_2Cu_3O_{6+x}$ (Y-123) the oxygen atoms are known to form chains in the CuO_x basal plane for $x \geqslant 0.35$,[1] causing a tetragonal-to-orthorhombic transition. These orthorhombic chain superstructures have been studied extensively by diffraction techniques[2–4] and a clear connection between the local oxygen configuration and T_c has been established.[5–7] The chain formation causes a substantial number of oxygen ions in the basal plane to have a nominal valence of O^- and a charge transfer of holes to the CuO_2 planes can occur[8] making the cuprate metallic and, eventually, superconducting.

While the structural phase diagram of pure Y-123 in the orthorhombic, superconducting state with $x \geqslant 0.35$ has been studied in detail both experimentally and theoretically[3,4,9,10] relatively few data exist on possible oxygen ordering in the other R-123 compounds.[11] The superconducting and antiferromagnetic phase diagram as function of oxygen doping has been studied for R-123 compounds with R=Y, Nd, La, Gd, and Tm by Lütgemeier *et al.*[12] At oxygen concentrations $x \geqslant 0.65$ $NdBa_2Cu_3O_{6+x}$ (Nd-123) and $LaBa_2Cu_3O_{6+x}$ (La-123) undergo a transition from a tetragonal insulating state to an orthorhombic superconducting state.[12,13] From nuclear quadrupole resonance measurements, Lütgemeier *et al.* suggest that the different behavior of T_N and T_c originates from other types of oxygen ordering taking place in the rare-earth compounds with ionic radii larger than Y. Inspired by this work, we have prepared single crystals of Nd-123 and La-123 with oxygen concentrations of $x \approx 0.4$, 0.5, and 0.76 and studied the samples by high-energy synchrotron x-ray diffraction. Distinct superstructure reflections related to oxygen ordering are observed in Nd-123 with $x \approx 0.5$, while no indications of oxygen ordering was detected in any other of the Nd-123/La-123 samples.

The samples were grown by a flux method in yttria stabilized zirconia crucibles.[14,15] They were prepared to the desired oxygen concentrations by a high-precision gasvolumetric technique as described in Ref. 16 using pure Y-123 powder as buffer material. The samples received an oxygen treatment optimized for Y-123.[17] Due to differences in equilibrium pressures for Nd-123/La-123 and Y-123,[18] we expect the actual oxygen content to be slightly smaller than the value aimed for (closer to $x \approx 0.47$). Three Nd-123 crystals with an oxygen concentration of $x \approx 0.5$ were investigated. One sample had a Nd substitution on the Ba site with a Nd:Ba ratio of 1.05:1.95, the other two samples were pieces from a crystal with a Nd:Ba ratio less than 1.04:1.96. These Nd/Ba ratios were estimated from the T_c of fully oxygenated samples.[19] The Nd-123 ($x \approx 0.5$ and 0.76) samples were investigated by ac susceptibility down to 4.2 K. In the $x \approx 0.5$ samples there were no indications of superconductivity, as expected, and the Nd-123 ($x \approx 0.76$) sample had a $T_c = 40$ K in good agreement with the $T_c(x)$ dependence found in Refs. 12 and 13.

The diffraction experiments were carried out with a photon energy of 100 keV at the dedicated high-energy wiggler beamline BW5 at the DORIS storage ring at HASYLAB. The beamline and the three-crystal diffractometer are described in Ref. 20. The high penetration power of the 100 keV photons makes it possible to perform diffraction experiments in horizontal Laue transmission geometry, probing the bulk of the sample. As monochromator and analyzer crystals, perfect Si(2 2 0) crystals were used for investigations of sample mosaicity and orthorhombicity. Imperfect $Si/TaSi_2$(1 1 1) crystals[21] were used for superstructure investigations. The samples were wrapped in Al foil and mounted in a small furnace centered on an Eulerian cradle. The furnace operating between room temperature and 250 °C is described in Ref. 4.

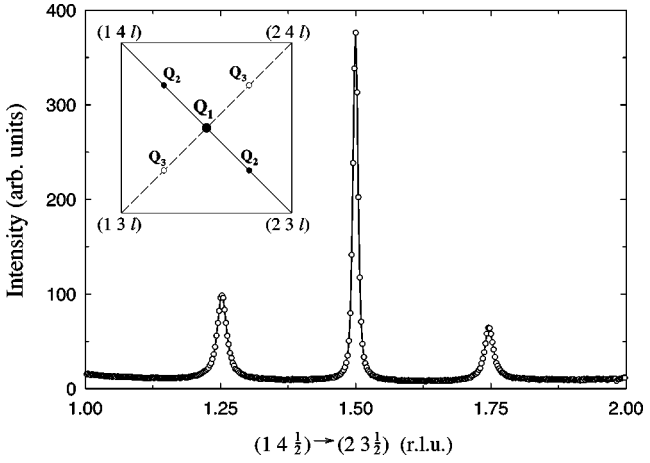

FIG. 1. (h k) scan in reciprocal space from (1 4 $\frac{1}{2}$) to (2 3 $\frac{1}{2}$) of the oxygen superstructure. Inset: the in-plane symmetry of the superstructure. The scan is probing the scattered radiation along the solid line through the $\mathbf{Q_1}$ and $\mathbf{Q_2}$ vectors.

The three Nd-123 samples prepared to $x \approx 0.5$ showed distinct superstructure reflections. The results from the samples were qualitatively the same, but the superstructure was much more pronounced in the samples with less Nd/Ba substitution, and the results will be shown for these samples only. None of the other La-123 and Nd-123 samples showed any sign of superstructure reflections despite careful scans along the axial and diagonal axes in reciprocal space. The in-plane peak width of the Nd-123 ($x \approx 0.5$) crystals determined from the (0 2 0) reflection was found to be $\Delta k = 3 \times 10^{-4}$ r.l.u. full width at half maximum (FWHM) and $\Delta h = 3 \times 10^{-4}$ r.l.u. FWHM, where r.l.u. is reciprocal lattice units. The longitudinal value (Δk) is limited by instrumental resolution[20] and gives a maximum orthorhombic splitting of $2(b-a)/(a+b) = 1.5 \times 10^{-4}$. The latter value corresponds to a sample mosaicity of 0.0086° or a maximum orthorhombic splitting as found from the longitudinal scan.

Superstructure reflections were found along the diagonals of the Brillouin zone, peaking at both integer and half-integer l as will be discussed in detail later. Despite careful search no reflections were found along any of the principal axes, unlike what is found for the orthorhombic superstructures in Y-123.[1–4] The intensity of the superstructure reflections was $\approx 10^{-4}$ of the fundamental Bragg peaks. The superstructures were found in all the zones of reciprocal space that were investigated, but most scans were performed in the zone spanned by the (1 3 l) and (2 4 l) vectors because there was only little overlap with the Al powder lines in this part of reciprocal space. Figure 1 shows a scan along the (1 4 $\frac{1}{2}$)→(2 3 $\frac{1}{2}$) diagonal, the inset shows the in-plane symmetry of the superstructure reflections.

The l dependence for the superstructures at (1.5 3.5 l), (1.75 3.25 l), and (1.75 3.75 l) is shown in Fig. 2. From the scans shown in Figs. 1 and 2 and supplementary scans (not shown here), we find that the symmetry of the superstructure reflections is described by three ordering vectors sketched in the inset to Fig. 1: $\mathbf{Q_1} = (\frac{1}{2}\ \frac{1}{2}\ \frac{1}{2})$, $\mathbf{Q_2} = \pm(\frac{1}{4}\ \frac{3}{4}\ n/2)$, $\mathbf{Q_3} = \pm(\frac{1}{4}\ \frac{1}{4}\ n/2)$ with n integer. The three ordering vectors have different peak intensities with $I_{Q_1} > I_{Q_2} > I_{Q_3}$. The $\mathbf{Q_1}$ reflections are fundamentally different from the $\mathbf{Q_2}, \mathbf{Q_3}$ reflections, with relatively narrow peaks at every half-integer l. $\mathbf{Q_2}$ and $\mathbf{Q_3}$ are much broader indicating a shorter correlation length, peaking at both integer and half-integer l. The in-plane profiles are all best fitted by Lorentzians. Along l the line shape of $\mathbf{Q_1}$ is Lorentzian while $\mathbf{Q_2}, \mathbf{Q_3}$ can only be fitted satisfactorily with Gaussians centered at half-integer and integer l. For all three ordering vectors the intensity variation follows approximately the same trend along l. There are some differences, however, most notably at $l = \pm 4.5$ where the $\mathbf{Q_1}$ and $\mathbf{Q_2}$ have maximum intensity while $\mathbf{Q_3}$ is extinguished. The temperature dependence of the superstructures is shown in Fig. 3. It was determined from h scans and l scans at $\mathbf{Q_1} = (1.5\ 3.5\ l)$, $\mathbf{Q_2} = (1.25\ 3.75\ l)$ and $\mathbf{Q_3} = (1.25\ 3.25\ l)$. For all three ordering vectors the intensity drops close to zero at 50 °C, but above 50 °C they behave differently. Noticeably, for all $\mathbf{Q}$ the correlation along the c axis persists well above 50 °C. This indicates that the correlation along c is quite (surprisingly) strong. Only $\mathbf{Q_2}$ displays discernible in-plane intensity above 50 °C, and while $\mathbf{Q_1}$ and $\mathbf{Q_3}$ are broadened above 50 °C the $\mathbf{Q_2}$ linewidth remains constant. The superstructure reflections did not return immediately when cooling to room temperature again, but after three days they had regained 10% of their intensities and the reflections were broadened by a factor of 3. Measurements after six months annealing at room temperature revealed that the superstructure intensity and half-widths had fully recovered.

The temperature dependence and long-time recovery at room-temperature annealing demonstrate that the diffuse reflections truly originate from oxygen ordering and not from lattice distortions or some impurity phase as, e.g., observed in some Y-123 samples.[22,23] The symmetry of the superstruc-

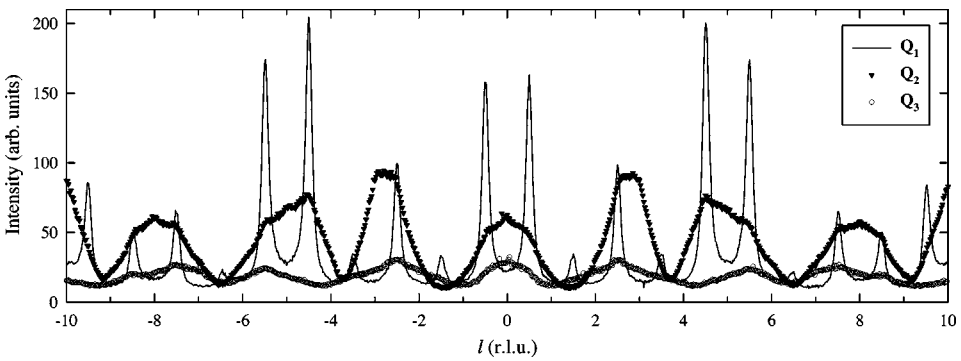

FIG. 2. l scan of the oxygen super-structures with ordering vectors $\mathbf{Q_1} = (1.5\ 3.5\ l)$, $\mathbf{Q_2} = (1.75\ 3.25\ l)$ and $\mathbf{Q_3} = (1.75\ 3.75\ l)$.

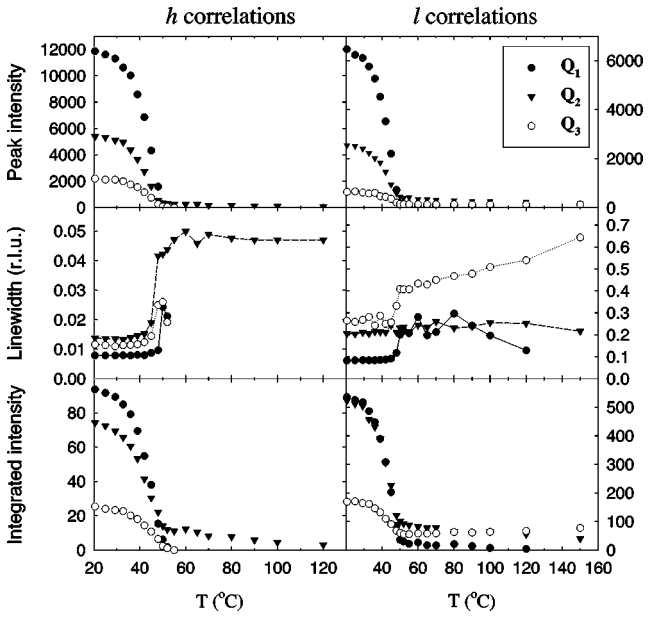

FIG. 3. Temperature dependence of intensity and linewidth FWHM for the three superstructure vectors determined in-plane (h) and out of plane (l).

ture reflections is different from the ''herringbone'' superstructure suggested in Ref. 12, as the two possible orientations of this structure can never give both the $\mathbf{Q_2}$ and $\mathbf{Q_3}$ reflections. The superstructure for Nd-123 was solved the following way:

First we consider the intensity modulation along l seen in Fig. 2. It is composed of peaks positioned at integer and half-integer l with amplitudes slowly varying with l in a similar way to that of the ortho-III and ortho-VIII superstructures in Y-123.[4,24] These variations have been shown to originate from the oxygen ordering and minor induced displacements of the oxygen atoms and the cations.[24] We neglect the slow intensity variations and analyze the possible oxygen ordering superstructures on fixed lattice sites from the selection rules of the ordering vectors.

The superstructure unit cell could easily be identified as $2\sqrt{2}a\times 2\sqrt{2}b\times 2c$ with $a=b$ in the tetragonal state. It is rotated 45° with respect to the basic crystallographic unit cell in the ab plane, and has a doubling of the c axis. Assuming an oxygen concentration of exactly $x=0.50$ and equal occupancy in each CuO_x plane, the diffraction patterns for all possible oxygen configurations within the given unit cell were calculated numerically.[25] By comparing the calculated reflections to the experimentally determined diffraction pattern it turns out that only three unique configurations exist that in combination reproduce the superstructure reflections. Details of the procedure are given in Ref. 26.

The $\mathbf{Q_1}$ originates from the oxygen configuration shown in Fig. 4(a). It is simply the square configuration with maximum distance between neighboring oxygen atoms shifted one unit cell along (1 0 0) from plane to plane along the c axis.

The selection rules for $\mathbf{Q_2}$ and $\mathbf{Q_3}$ are only fulfilled for two different configurations which we shall refer to as the ''small squares'' and ''ragged stripes'' [see Fig. 4(b)]. The ''small squares'' give reflections at both $\mathbf{Q_2}$ and $\mathbf{Q_3}$, while

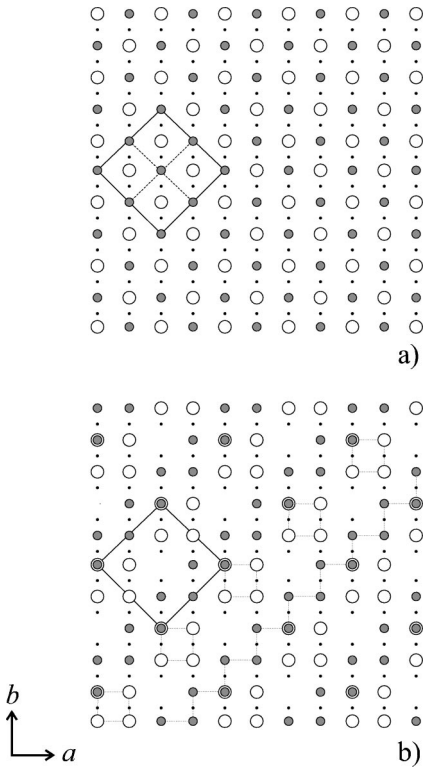

FIG. 4. Oxygen configurations belonging to the $\mathbf{Q_1}$ vector (a) and to the $\mathbf{Q_2}$ and $\mathbf{Q_3}$ vectors (b). The small filled circles are Cu atoms, the large circles are occupied oxygen sites. White and shaded atoms are shifted along the c axis by one unit cell with respect to each other, and oxygen atoms overlapping along the c axis are shown as concentric white and shaded circles. The superstructure shown in (b) is a combination of alternating ''small squares'' (white atoms) and ''ragged stripes'' (shaded atoms) configurations, outlined with dotted lines as a guide to the eye. Solid lines show the superstructure unit cell in the ab plane. For (a) the unit cell can be further subdivided as indicated by the dashed lines. Configurations with the oxygen atoms on the a axis are equally possible.

''ragged stripes'' along the (1 1 0) and (1 $\bar{1}$ 0) directions contribute to $\mathbf{Q_2}$ and $\mathbf{Q_3}$, respectively. These configurations should be stacked along the c axis to give reflections at both integer or half-integer values of l. A prerequisite for reflections at integer values of l is that two consecutive sites along the c axis in the $2\sqrt{2}a\times 2\sqrt{2}b\times 2c$ unit cell are occupied. These requirements can be accomplished for configurations with only ''small squares'' that overlap on two sites, and for alternating layers of ''ragged stripes'' in the (1 1 0) and (1 $\bar{1}$ 0) directions, but the intensity and l modulation at $\mathbf{Q_2}$ and $\mathbf{Q_3}$ would then be identical, which is not observed experimentally (see Fig. 2). The simplest combination with minimal overlap of oxygen atoms along the c axis giving the $\mathbf{Q_2}$ and $\mathbf{Q_3}$ peaks is shown in Fig. 4(b). If the ''small squares'' and ''ragged stripes'' configurations are shifted by an in-plane lattice vector relative to each other, there can be an overlap of three occupied oxygen sites along c within the superstructure unit cell. This will increase the intensity at integer l relative to that at half integer, but not affect the symmetry in the (h k) plane. The broad features of the $\mathbf{Q_2}$,$\mathbf{Q_3}$ reflections shown in Fig. 2 indicate that we do not have an ideal stacking as depicted in Fig. 4(b) but rather a

more or less random stacking of the two ''square'' and ''stripe'' configurations. Assuming that the configurations in Fig. 4(a) and (b) occupy equally large volumes in the sample and considering scattering from oxygen atoms alone, a direct calculation of the structure factor from the configurations will give peak intensity ratios $I_{Q_1}:I_{Q_2}:I_{Q_3}\simeq 16:5:1$ which reproduces fairly well the ratios shown in Fig. 2.

The configuration of ''ragged stripes'' in Fig. 4(b) are running along the (1 1 0) direction. For a tetragonal crystal we would expect just as many ''ragged stripes'' along the $(1\,\bar{1}\,0)$ direction and thereby essentially the same intensity at $\mathbf{Q_2}$ and $\mathbf{Q_3}$ positions. However, since the $\mathbf{Q_2}$ reflections are strongly dominating the $\mathbf{Q_3}$ reflections in Fig. 2, we must conclude that the ''ragged stripes'' run predominantly in the (1 1 0) direction. We suggest that this preference is a sample dependent feature similar to the higher density of certain orthorhombic twin domains observed in Y-123. The tetragonal symmetry is not violated provided that the average oxygen occupation on the *a* and *b* axes are equal. We suggest that strain fields associated with the ideal configurations shown in Fig. 4 with oxygen occupation exclusively on the *b* axis and with overlap along the *c* axis contribute to the finite size in-plane ordering and weakly correlated sequences of ''small squares'' and ''ragged stripes'' configurations along the *c* axis.

The oxygen ordering in Y-123 has been studied theoretically within the ASYNNNI model[9] which explains the chain-like structures along the *b* axis in this material by three effective interaction parameters: a strongly repulsive nearest-neighbor interaction, V_1, and two next-nearest-neighbor interactions, of which a relatively strong attractive V_2 is mediated via the Cu atoms, and a weaker repulsive one, V_3, is without intermediate Cu. Wille and de Fontaine[27] have analyzed the ASYNNNI model for $x=0.5$ and found that the $\mathbf{Q_1}$ and the ''small squares'' configurations are stabilized within this model for V_2 and V_3 both being repulsive or attractive, respectively. They also predict that other structures may be stable if interactions of longer range are included as has proven to be necessary for Y-123.[10] The effective interaction parameters in the ASYNNNI model have been calculated from first-principles total-energy calculations for Y-123 (Ref. 28) but not for Nd-123. The lattice parameters of Nd-123 are somewhat larger than in Y-123 and the interaction parameters may therefore be changed. However, it appears unlikely that the complex oxygen-ordering properties of Nd-123 may be explained within a simple extension of the ASYNNNI model.

For the type of oxygen configurations of $NdBa_2Cu_3O_{6.5}$ determined in this work there are no chains longer than two consecutive oxygen atoms, or any clustering in domains of appreciable size. We shall emphasize that if the two assumptions hold ($x=0.5$, equal occupancy in all CuO_x planes) the combination of ''small squares'' and ''ragged stripes'' visualized in Fig. 4(b) combined with the $\mathbf{Q_1}$ configuration in Fig. 4(a) represents the only possible solutions to the experimental data. These configurations are not able to act as electron acceptors,[5,7,8] and the superstructures are thus unlikely to give rise to any charge transfer to the CuO_2 planes. This demonstrates unambiguously that the different $T_c(x)$ behavior for Y-123 and Nd-123 originates from different oxygen ordering in the two compounds.

This work was supported by the Danish Technical Research Council and DANSYNC. We are also grateful for financial support from HASYLAB.

[1] C. Chaillout *et al.*, Phys. Rev. B **36**, 7118 (1987).
[2] R. Beyers *et al.*, Nature (London) **340**, 619 (1989).
[3] N. H. Andersen *et al.*, Physica C **317-318**, 259 (1999).
[4] M. v. Zimmermann *et al.*, cond-mat/9906251 (unpublished).
[5] R. J. Cava *et al.*, Physica C **165**, 419 (1990).
[6] J. D. Jorgensen *et al.*, Physica C **167**, 571 (1990).
[7] H. F. Poulsen *et al.*, Nature (London) **349**, 594 (1991).
[8] G. Uimin and J. Rossat-Mignod, Physica C **199**, 251 (1992).
[9] D. de Fontaine *et al.*, Phys. Rev. B **36**, 5709 (1987).
[10] D. Mønster *et al.*, Phys. Rev. B **60**, 110 (1999).
[11] T. Krekels *et al.*, Physica C **196**, 363 (1992).
[12] H. Lütgemeier *et al.*, Physica C **267**, 191 (1996).
[13] G. Flor *et al.*, Physica C **316**, 13 (1999).
[14] T. Wolf *et al.*, Phys. Rev. B **56**, 6308 (1997).
[15] T. Wolf *et al.*, J. Cryst. Growth **96**, 1010 (1989).
[16] N. H. Andersen *et al.*, Physica C **172**, 31 (1990).
[17] Samples of ≈10 g Y-123 powder at full oxidation ($x\approx 1$) and the crystals were annealed at 550 °C in a closed gasvolumetric system until the oxygen content had been reduced to the desired value. The samples were isolated in a small volume to prevent oxygen uptake and the temperature was reduced in one step to 350 °C followed by cooling to room temperature at 7 °C/hour.
[18] T. B. Lindemer *et al.*, Physica C **255**, 65 (1995).
[19] H. Shaked *et al.*, Phys. Rev. B **41**, 4173 (1990).
[20] R. Bouchard *et al.*, J. Synchrotron Radiat. **5**, 90 (1998).
[21] H. B. Neumann *et al.*, Nucl. Instrum. Methods Phys. Res. A **372**, 551 (1996).
[22] A. Bertinotti *et al.*, Physica C **160**, 227 (1989).
[23] F. Yakhou *et al.*, Physica C **261**, 315 (1996).
[24] A. Stratilatov *et al.*, Phys. Lett. A **180**, 137 (1993).
[25] By definition the first site in the first plane is always occupied. This gives 455 combinations in the first plane and 1820 in the second. The limited number of combinations, 828 100 in total, makes it feasible to systematically calculate the structure factor for all the combinations.
[26] T. Frello, Ph.D. thesis, Risø National Laboratory, 1999. Available at http://www.risoe.dk/rispubl/FYS/ris-r-1086.htm
[27] L. T. Wille and D. de Fontaine, Phys. Rev. B **37**, 2227 (1988).
[28] P. A. Sterne and L. T. Wille, Physica C **162-164**, 223 (1989).